Horizontal variability of surface currents in the Dead Sea

Dead Sea
HF radar
Surface currents

Mer Morte
Radar HF
Courants de surface

Heinz-H. ESSEN [a*], Klaus-W. GURGEL [a], Florian SCHIRMER and Ziv SIRKES [b]

[a] Universität Hamburg, Institut für Meereskunde, Troplowitzstr. 7, D 22529 Hamburg, Germany.

* Presently at Saclant Undersea Research Centre, Viale San Bartolomeo 400, 19138 La Spezia, Italy.

[b] Center for Ocean and Atmospheric Modelling, Stennis Space Center, Building 1103, MS 39529, USA.

Received 28/06/94, in revised form 17/01/95, accepted 03/02/95.

ABSTRACT

Surface currents in the Dead Sea, as measured by two land-based HF (high frequency) radar stations in autumn 1984, are analysed. High horizontal variability is observed, which may partly be explained by the inhomogeneous wind field. Decomposition into empirical orthogonal eigenfunctions (EOF) shows that the currents may not be represented by a small number of patterns. The forcing of currents by wind is proved through significant correlation between both. Spatially-averaged rotary spectra provide evidence of the presence of inertial oscillations. The data set allows the calculation of horizontal derivatives. Time series of divergence and curl are presented. By estimating the advective terms of the Navier-Stokes equation it is shown that nonlinear effects are important.

RÉSUMÉ

Variabilité horizontale des courants de surface en Mer Morte.

Les courants de surface en Mer Morte mesurés par deux stations radar HF terrestres en automne 1984 sont analysés. La grande variabilité horizontale observée est en partie expliquée par les inhomogénéitiés du champs de vent. La décomposition sous forme de fonctions propres orthogonales empiriques (EOF) montre que les courants ne peuvent pas être représentés par un nombre réduit des modes. Le forçage par le vent est prouvé par une corrélation significative entre vent et courants. Les spectres rotatifs moyennés spatialement mettent en évidence la présence d'oscillations d'inertie. Les données permettent le calcul des dérivées horizontales. Les distributions temporelles de la divergence et de la vorticité sont présentées. En estimant les termes d'advection de l'équation de Navier-Stokes, il est montré que les termes non-linéaires sont importants.

Oceanologica Acta, 1995, **18**, 4, 455-467.

INTRODUCTION

During autumn 1984, the Weizmann Institute of Science (Israel) and the Institut für Meereskunde at the University of Hamburg (Germany) performed a joint experiment in the Dead Sea. Part of the investigations involved the monitoring of sea-surface currents by means of a Coastal Radar (CODAR). This system yields mean current velocities, averaged vertically over about the first 0.5 m, horizontally within some 10 km^2, and over a time of 18 min. Two radar stations at locations some 20 km apart (each measuring radial current speeds) are necessary to construct the two-dimensional vectors, which are then available on a grid of 1.5 km spacing in the Dead Sea. For the performance of

CODAR the water has to be conductive, *i.e.* salty. Only a few inland seas in the world fulfill this requirement. For this reason, the data set presented here can be considered to be unique.

The Dead Sea is located in the Jordan Rift Valley, at the lowest point on the surface of the earth, more than 400 m below sea level. It has two basins, a large northern and a smaller southern one, which has now dried out. The topography around the Dead Sea is very ragged. The peaks of the surrounding mountains reach 1150 m above mean sea level. The sea is located in a channel with many dry river beds. Its length is 50 km and its width at most 17 km. Its average depth is 180 m, the maximal depth nearly 330 m. Its salinity at the time of our measurements was 27.7 % and its density 1.236 g/cm^3. Since the Dead Sea has no outflow, evaporation is the only mechanism by which it loses water.

Sirkes (1986, 1987) analysed sea-level fluctuations in the Dead Sea from summer 1981 and autumn 1984. The spectral analysis of the summer data, when the Dead Sea was stratified, revealed peaks at frequencies which correspond to the periods of 24 h and those of internal seiches. These peaks were not present in the autumn data, where the vertical density stratification was homogeneous. The differences in sea-level time series for summer 1981 and autumn 1984 are due not only to different stratifications but also to different wind regimes. During summer there is a very constant diurnal wind in the north-south direction, whereas the wind pattern in autumn is irregular. This irregularity strongly influences the surface currents, as Sirkes (1986) discussed by means of selected CODAR maps. In a more concentrated form, these results are presented in a book article by Sirkes *et al.* (1995).

Essen (1993) investigated the forcing of (CODAR-measured) surface currents by wind in different areas of the Baltic and the North Sea, and included also some data from the Dead Sea. With respect to the correlation and the veering of current against wind direction, he found evidence for Ekman-type currents in all the areas considered. Because of the uniqueness of the CODAR data set from the Dead Sea, the authors decided to continue with the analysis, placing more emphasis on the horizontal variability. After long periods of interruption, this work now came to a certain end.

Surface currents in the Dead Sea are obviously driven by wind. By means of the method of vector correlation it has been found that about 45 % of the current variance can be explained by linear wind-forcing, and the current turns to the right by 11 degrees against the wind. These results refer to a position close to the coast, where reliable wind data were available, but the current may be affected by the topography or could be remotely driven. The maps of surface currents are very complex, somehow random-like. The attempt at identifying a few dominant patterns by means of decomposition into empirical orthogonal eigenfunctions (EOFs) was not very successful, except for the first EOF. This appears to be rather homogeneous and accounts for 53 % of the variance of surface currents, *i.e.* in all likelihood contains the response to changes of the mean wind field.

Spectral analysis of the time series available has been performed. In order to increase the statistical significance, the spectra of the current velocity have been averaged over all grid points. For both wind and current, no diurnal peak could be found. Rotary spectral analysis reveals the presence of inertial waves. Clockwise rotating currents account for the predominant portion of variance around the inertial period. The broad peak may be explained by the assumption that these oscillations are relatively short events.

The CODAR data permit the computation of horizontal derivatives and deduced values like divergence and curl. In addition, the acceleration terms in the Navier-Stokes equation can be determined and compared with each other. In order to assess the accuracy of the results, some emphasis has been laid on the estimation of errors. To obtain reliable horizontal derivatives, averaging has to extend over some 5 km to 10 km in both coordinates. In general, the values of curl and divergence are considerably smaller than f. A period of downwelling in the southern Dead Sea could be identified, which coincides with strong south-directed currents. Comparing the acceleration terms it may be concluded that generally the linear terms, *i.e.* the temporal and Coriolis acceleration, exceed the advective (nonlinear) terms. But the dominance is not so strong that nonlinear effects can be neglected.

MEASUREMENTS

CODAR was developed for measuring surface currents in coastal areas. The physics behind the system is Bragg scattering. An electromagnetic wave is backscattered from surface waves of half its wavelength running towards or away from the radar site. The Doppler shift of the received signal is determined by the phase velocity of the scattering surface wave, which is known from the dispersion relation. Deviations from this theoretical value are assumed to be due to underlying currents. A detailed discussion of the theoretical background and the realization of the measuring system of CODAR is given by Barrick *et al.* (1977).

The CODAR of the University of Hamburg is a modified version of that developed by Barrick *et al.* (1977), and has been successfully operated in a number of experiments in the Baltic and North Seas (Essen *et al.*, 1984; Essen *et al.*, 1988; Essen *et al.*, 1989). The frequency used is 29.85 MHz, corresponding to a wavelength of about 10 m. One CODAR site measures radial current speeds with respect to its position. Two distinct sites are necessary to obtain two-dimensional current vectors. In general, the range of each site is between 30 km and 50 km, mainly depending on sea state. Though the surface of the Dead Sea sometimes looked very calm, we always obtained return signals, but in a few cases the ranges were limited to 20 km. The two CODAR stations were located at Kidron and Ein-Gedi (KI and EG in Fig. 1, respectively). In order to obtain a high spatial resolution (1.2 km), 8 μs transmit pulses were used instead of 16 μs pulses as in the experiments mentioned above.

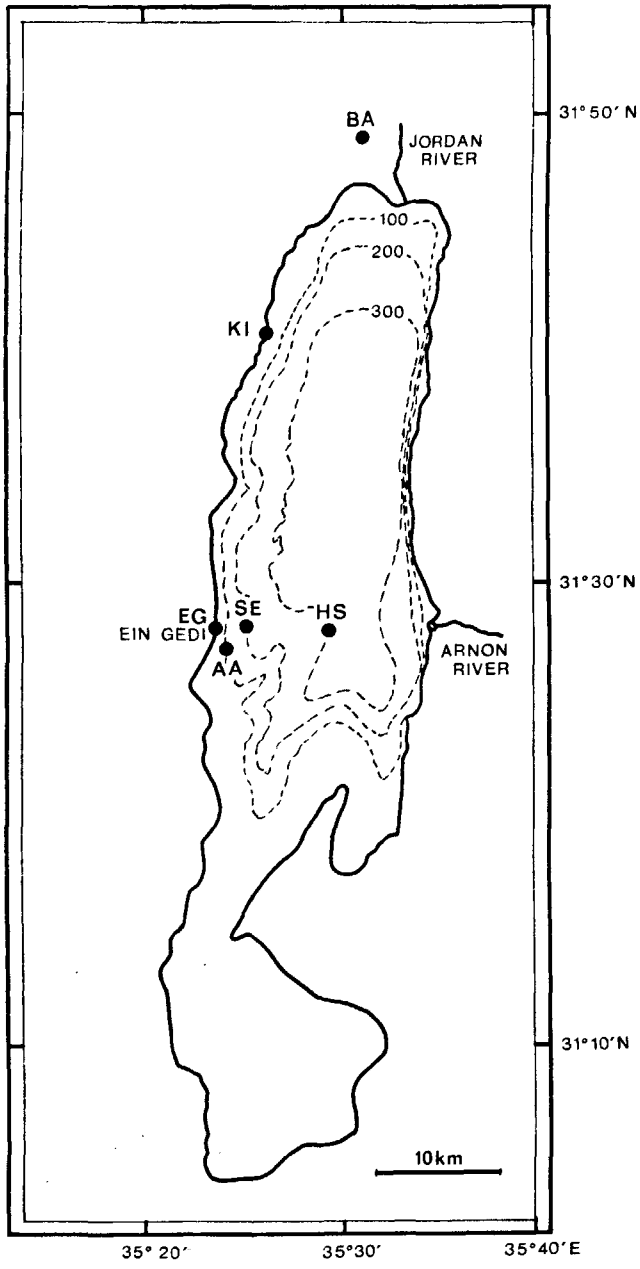

Figure 1

Map showing the bathymetry of the Dead Sea and the locations of measurements: Beit-Ha'arava (BA), Kidron (KI), Ein Gedi (EG), floating station (SE), Aanderaa mooring (AA), hydrographic station (HS). The depth contours are in metres and refer to the lake surface.

The CODAR measurements were carried out over nine days, at least twelve times a day. The obtained current velocities are mean values, averaged over 18 min in time (measuring time), vertically over about 0.5 m from surface (as deep as the scattering waves "feel" currents), and horizontally within a circle of 2 km radius (depending on pulse length and processing algorithms). Each CODAR measurement yields a map of two-dimensional currents.

Figure 1 shows the geography and bathymetry of the Dead Sea. Measurements at the different locations indicated were carried out between 24-Nov. and 2-Dec. 1984. In the morning of 27-Nov. a temperature profile was taken off Ein-Gedi in the central lake (HS in Fig. 1) and water samples from different depths were collected for analysis of their salinity (Anati, 1984). From these two types of measurements it was found that the vertical density stratification down to 60 m was homogeneous. This finding is in accordance with the fact that surface-level measurements showed no indication of the presence of internal seiches, in contrast to observations in summer 1981, *cf.* Sirkes (1986, 1987).

Winds are measured routinely by different institutions at several locations on the western shore of the Dead Sea and at one station in the sea, which are are indicated in Figure 1: Beit Ha'arava (BA), Kidron (KI), Ein Gedi (EG), sea station (SE). All measurements were taken 3 m above ground except the measurements at sea, which were taken 7 m above sea surface. Time series of wind from the four stations are displayed in Figure 2. Despite the obvious correlation it may be stated that there are considerable differences in the wind patterns and the wind field cannot considered to be homogeneous over the sea. It is most likely that these differences are caused by the ragged topography around the Dead Sea.

Figures 3-4 show examples of current maps. A more detailed discussion of these maps than that presented here is given by Sirkes (1986). Mean current velocities, as defined above, are represented by arrows centred at the respective grid points. The grid distance is 1.5 km. That means, adjacent current vectors are not independent of each other, as

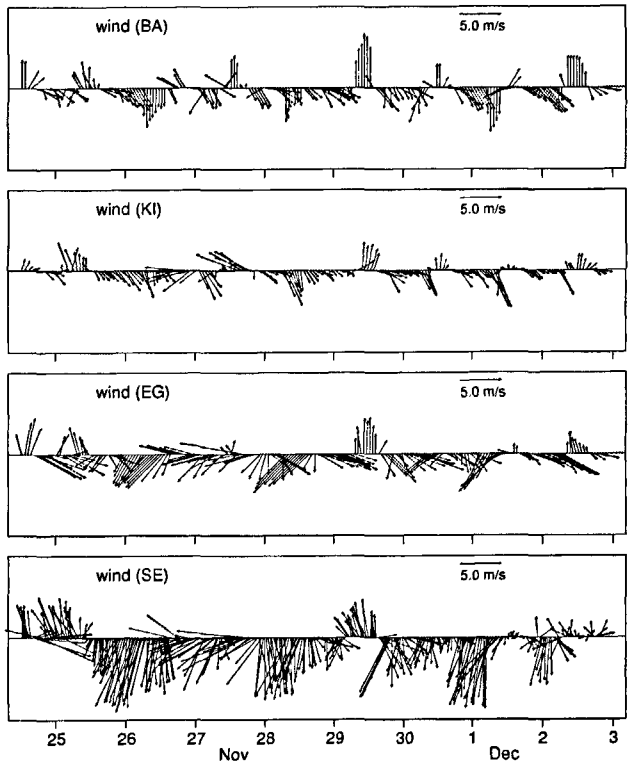

Figure 2

Time series of wind vectors (stick plot). The measuring positions are given in Figure 1, times are in UTC.

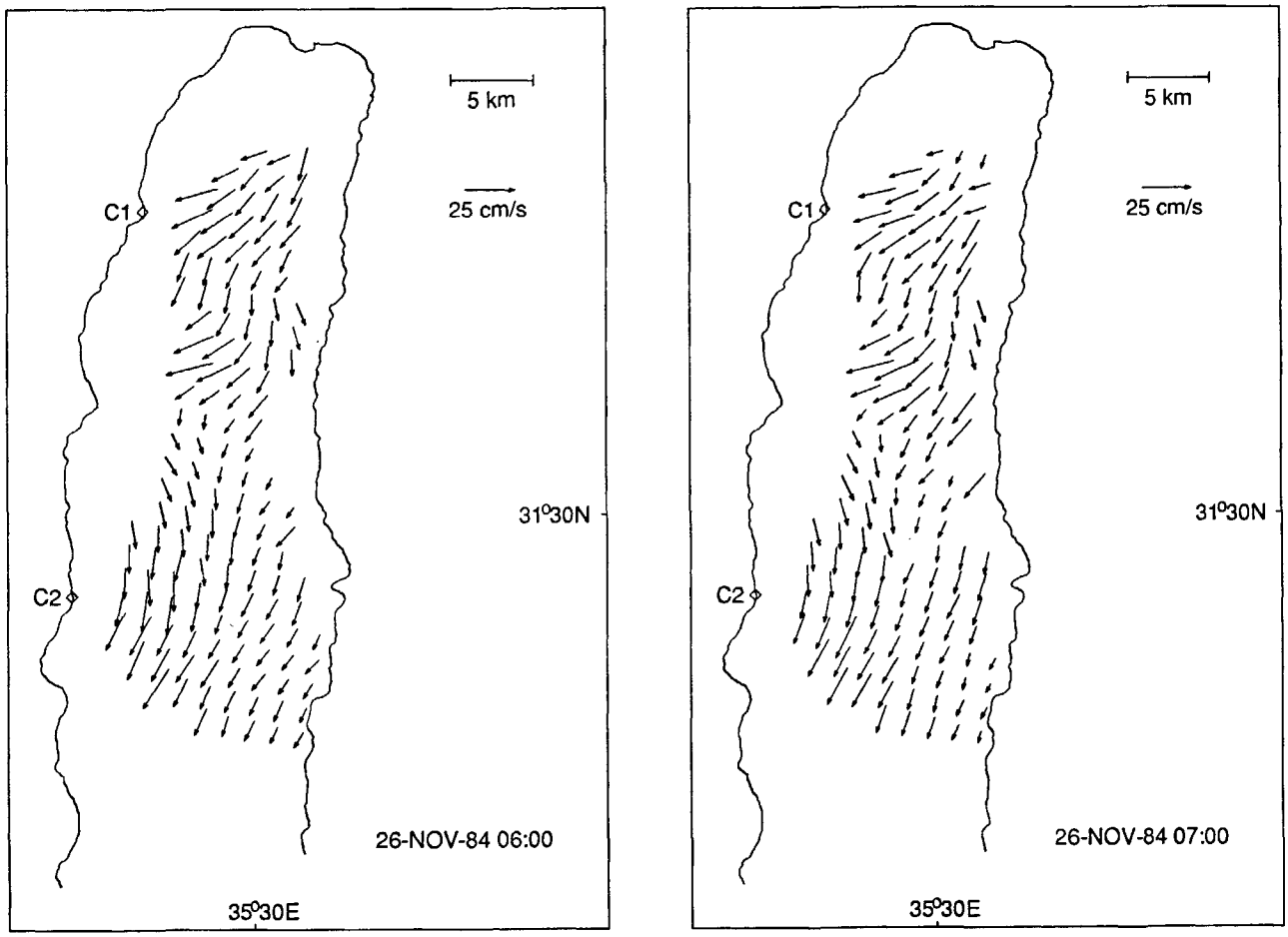

Figure 3

Examples of two-dimensional current fields, as measured by CODAR in the Dead Sea. Positions of the CODAR sites are marked by diamonds (C1 and C2). Vectors, representing the current velocity, are centred at the grid points with 1.5 km spacing.

there is some overlap of the averaging areas. Figure 3 shows the typical circulation pattern in the Dead Sea during the first three days of our measurements, with two different flow regions in the northern and southern part of the sea. While the south-south-westerly directed currents in the south are relatively stable, the currents in the north change direction continuously in clockwise direction. The two maps presented are separated by one hour and show only slight changes over this period. The two maps in Figure 4 are separated by six hours. During this time the flow pattern has changed completely, obviously due to an abrupt change in wind direction, *cf.* Figure 2.

In addition to the surface currents, as mapped by CODAR, sub-surface currents have been measured by means of moored Aanderaa current meters at 5 m and 10 m depth (AA in Fig. 1), *i.e.* close to the floating station. During the measuring period the current meters became increasingly covered by salt, which led to a standstill of the rotor at 10 m depth after 150 h of operation. Figure 5 displays the wind at the floating station (7 m above sea surface), current velocities as measured by CODAR at this location and the sub-surface currents from the current meters. Wind and sub-surface currents have been sampled every 1/2 h. The CODAR measurements are available with different sampling: 1 h and 2 h and some data lacking because of system failures and unsufficient radar propagation conditions. The temporal averaging is about the same for both current-measuring systems, 18 min for CODAR and 30 min for the current meters.

WIND-DRIVEN CURRENTS

Currents in the Dead Sea are driven by wind. For the measuring period in autumn 1984 the winds have been rather variable, both in time and space. The complex structure of the current fields, as observed in the CODAR maps, is partly due to winds but other influences also have to be considered, like the topography or the earth rotation. These influences are investigated by means of time-series analysis. The vector correlation between current and wind and currents at different depths is discussed. Variance spectra of current and wind are compared, and a two-dimensional EOF-analysis is performed.

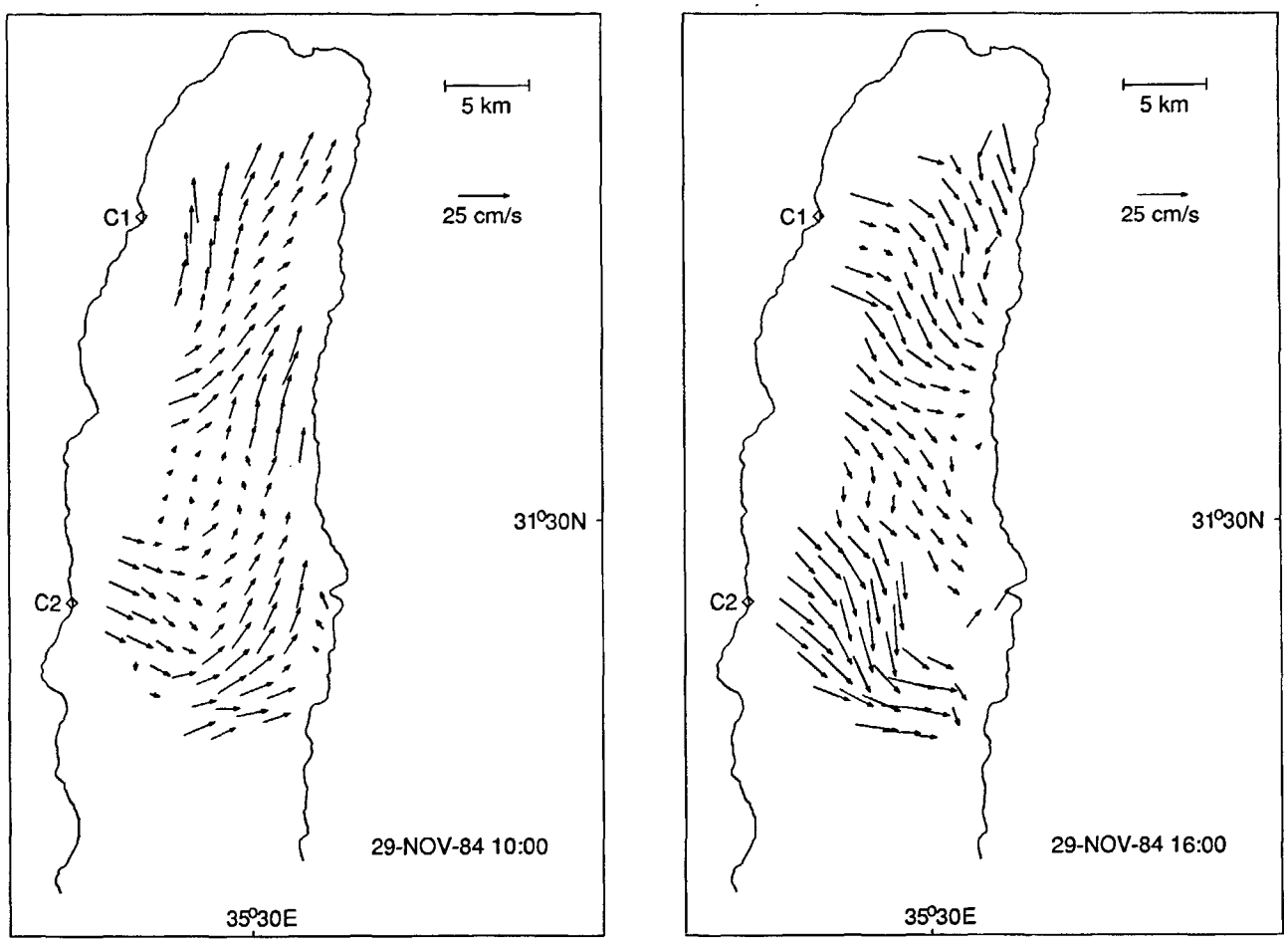

Figure 4

Same as Figure 3.

Vector-correlation

The time series of wind and current are available in terms of two-dimensional horizontal vectors, which are represented by complex numbers,

$$w_i = v_i + iu_i = |w_i| \exp(i\vartheta_i) \quad (1)$$

where v_i and u_i are the north- and east-component, respectively, and i counts the time. With this notation, the angles ϑ_i count clockwise from north. For the following analysis it is assumed that the time series are of zero mean, *i.e.* the mean has been subtracted.

The linear dependence of two complex time series may conveniently be investigated by means of vector correlation, which also determines the angle between the vectors correlated most strongly. This method is based on Kundu and Allen (1976) and has been applied to CODAR measurements from different areas by Essen (1993). In order to account for a possible delay of currents against wind, we consider a time lag between the time series. The complex cross-correlation function is defined by,

$$\rho_n = |\rho_n| \exp(i\varphi_n) = \sum_i w_{1i+n} w_{2i}^* / \left(\sum_i |w_{1i}|^2 \sum_i |w_{2i}|^2\right)^{1/2} \quad (2)$$

where *n* is the time lag in terms of the sampling interval. The asterisk denotes the complex conjugate and the sums are taken over all measurements available. φ_n is the mean angle between the vector series. In the case of identical time series, *i.e.* $w_{1i} = w_{2i}$, the above formula describes the auto-correlation function, which is real and symmetric around zero time lag.

In addition to the correlation function we also discuss the regression coefficient (at zero time lag),

$$r_0 = |r_0| \exp(i\varphi_0) = \sum_i w_{1i} w_{2i}^* / \sum_i |w_{2i}|^2 \quad (3)$$

the magnitude of which describes the mean ratio of amplitudes of the two time series, and φ_0 is the same as in (2).

Figure 6 (upper part) displays the auto-correlation functions of the time series under consideration, based on 1/2-hourly sampling. The missing CODAR data have been substituted by means of cubic spline interpolation. For a time lag up to 6 h, the auto-correlation function shows similar behaviour for all time series. The different shape of the CODAR auto-correlation around zero is an artifact of the spline interpolation and not real. As a result, we find currents to have approximately the same correlation time

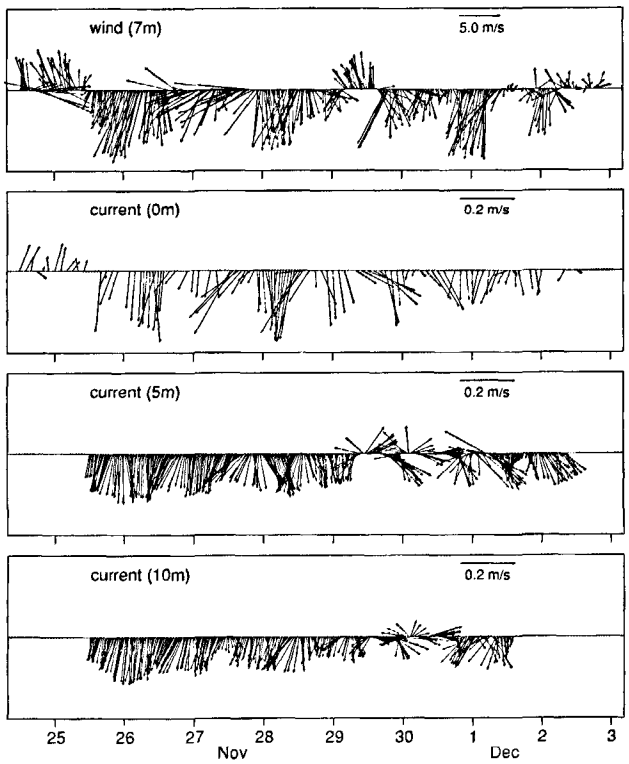

Figure 5

Vector-time series of wind (7 m above surface), surface currents measured by CODAR (both at position SE in Fig. 1), and sub-surface currents at 5 m and 10 m depths as measured by Aanderaa current meters (position AA in Fig. 1).

as wind. At larger time lags, the winds show some diurnal periodicity at 24 h and the currents around 15 h.

From Figure 5 a strong correlation between the different time series may be expected. But this mainly applies to the mean direction. Winds blowing towards the south dominate and drive surface currents in the same direction. By subtracting the means from the time series, a considerable part of the correlation is lost. Figure 6 (lower part) displays the magnitudes of all possible cross-correlation functions, *i.e.* $|\rho_n|$ as defined by (2). Except for the currents at 5 m and 10 m, the cross-correlations have flat structures near zero lag, and no general statement can be made about time lags. Surface currents seem to follow the wind without delay, *i.e.* with a lag not larger than resolvable (1 h).

In Table 1 the complex regression coefficient and the correlation coefficient (*i.e.* the respective function at zero time lag) are summarized. With respect to the CODAR measurements no interpolated data are used and the results differ slightly from those in Figure 6. The probabilty distribution of ρ_0, as absolute value of a complex number, is not the same as that of the correlation coefficient of real time series. A 95% limit for the hypothesis of zero correlation has been determined empirically from a great number of time series of uncorrelated normal-distributed random numbers. For the measured time series we assumed a correlation time of 5 h, estimated from the auto-correlation functions in Figure 6, and obtained M = 30 statistically

Table 1

Magnitude $|r_0|$ *and veering* ρ_0 *of the complex regression coefficient (3), and absolute value (at zero time lag)* $|\rho_0|$ *of the complex auto-correlation for time series of wind and current. M = estimated number of independent measurements,* ρ_G *= 95% limit for zero correlation.*

w_1[m/s]	w_2[m/s]	$\|r_0\|$	φ_0[deg]	$\|\rho_0\|$
cur (0)	wind	0.016±0.004	11±11	0.65
cur (5)	wind	0.010±0.004	−29±22	0.43
cur (10)	wind	0.006±0.003	−22±25	0.34
cur (5)	cur (0)	0.42±0.17	−30±18	0.46
cur (10)	cur (0)	0.21±0.12	−15±29	0.30
cur (10)	cur (5)	0.54±0.18	−5±8	0.46
		M = 30 , ρ_G = 0.32		

independent data for the series of 150 h duration. The respective limit ρ_G for zero correlation is presented in Table 1. It may be concluded that there is a significant correlation between the time series, except for currents at 10 m depth against wind as well as surface currents.

Considering the north- and south-component separately, it transpires that most of the correlation is due to the north component (parallel to the coast). The same applies to the correlation of wind and sub-surface current. The relatively low correlation of surface and sub-surface current may be

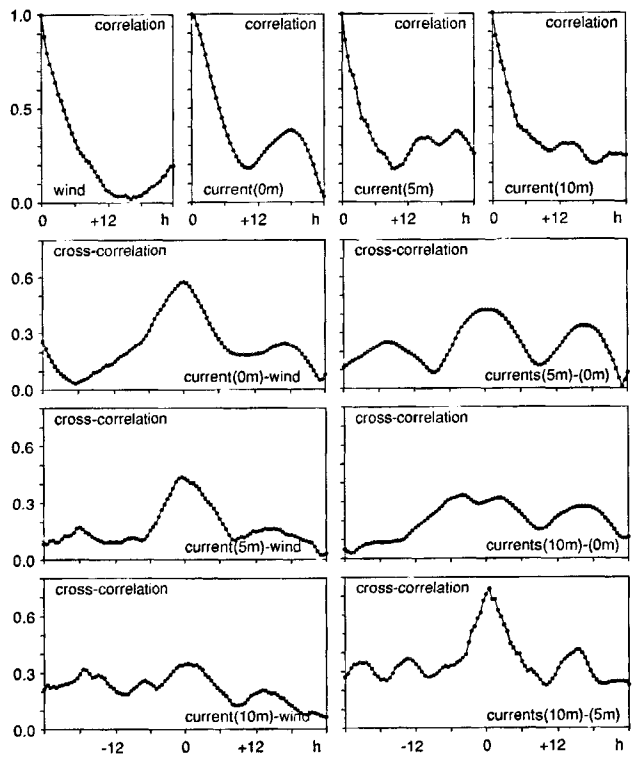

Figure 6

Auto-correlation functions (upper panels) and magnitudes of the complex cross-correlation functions of wind and current at different depths, from the time series of Figure 5.

explained by the different quantities they represent. While the CODAR data are spatial means over a horizontal circle of 2 km radius and a vertical layer of about 0.5 m, the current meters perform point measurements. Because of horizontal variability, these values may differ considerably. The highest correlation in Table 1 is that between surface current and wind, which indicates that 42 % (squared correlation coefficient) of the surface-current variance is due to linear wind forcing.

The standard deviations of $|r_0|$ and φ_0, as given in Table 1, have been determined from the covariance matrix of the complex regression coefficient r_0, using the linearized equations describing the dependence of $(|r_0|, \varphi_0)$ on r_0 in the vicinity of the respective quantities. The covariance matrix of r_0 has been estimated from the measured data.

The value of $|r_0|$ represents the current-to-wind ratio or the decrease of currents with depth, respectively. With respect to surface currents the current-to-wind ratio is 0.016. Again, for the north component only, we find the higher value of 0.019, which is in good agreement with values measured in the North Sea and the Baltic (Essen, 1993). This result is not evident because of the high salinity of Dead Sea water. As expected for wind-driven currents, their amplitudes decrease with depth. Regarding wind-stress instead of wind-velocity, the above analysis yields similar results with about 10% lower correlation to surface currents but the same correlations to sub-surface currents.

According to Ekman's theory the angle φ_0, which describes the rotation of the first vector against the second, should be positive in all the cases investigated in Table 1. In the northern hemisphere currents should turn to the right from wind, and rotate clockwise with increasing depth. In fact, φ_0 is only positive for wind-driven surface currents. The discrepancy for the other cases may be explained by the position of the current meters close to the coast on a strongly sloping bottom, *i.e.* the influence of topography. In addition, the veering angles should be interpreted with caution because of their high standard deviations.

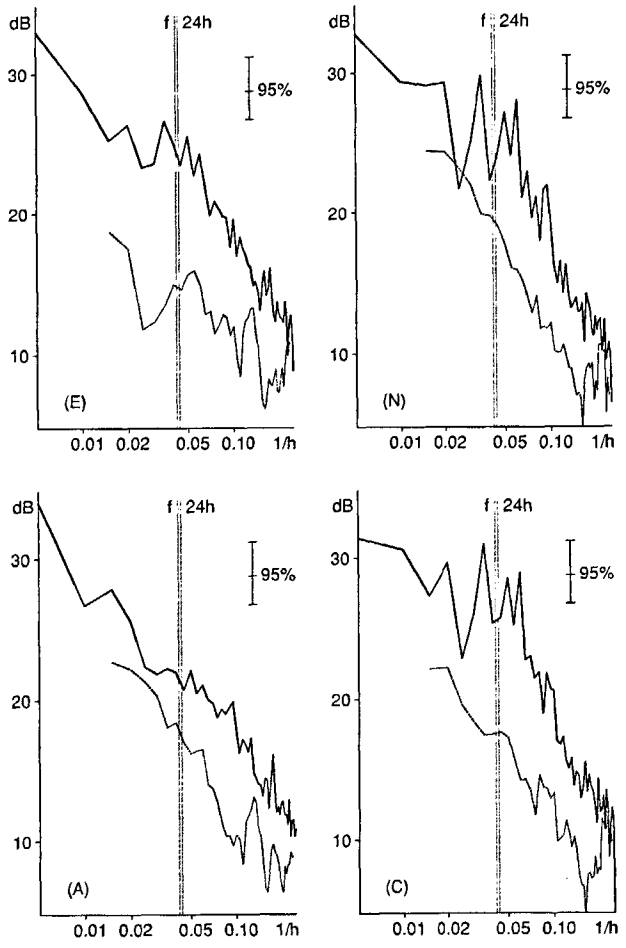

Figure 7

Spectral variance of current (bold lines) and wind (thin lines). The upper panel displays east-(E) and north-component (N), the lower panel rotary spectra with anti-(A) and clockwise (C) rotating components. The dB-scale refers to (1 cm s^{-1})^2 in the case of currents and to (1 m s^{-1})^2 in the case of winds. The current spectra represent an average over 75 grid points, the wind spectra are from a single time series smoothed by a moving average over five adjacent frequencies. The confidence limits are valid for the currents only. The 24 h and the inertial period f are indicated by vertical lines.

Variance spectra

Frequency analysis of the single time series available at a given position suffers from the limited length and the corresponding high variance of spectral estimation. Considering the time series at different grid points as part of the same ensemble, more accurate estimations may be obtained by averaging the different spectra. The variance spectra of both components of surface currents and the rotary spectra in Figure 7 are computed from 75 grid points, covering the whole sea. Some statistical dependence of the data, due to the overlap of averaging areas and horizontal correlation, has to be taken into consideration. From the investigation of horizontal correlation lengths, it may be concluded that a number of 30 degrees of freedom (*i.e.* 15 independent grid points) is a reasonable value.

Because of the data available, variance spectra of wind refer to single time series, only. In order to suppress the high spectral variance, a running mean over five adjacent spectral lines has been taken, which reduces the spectral resolution. Wind spectra from the three land stations and the floating station are quite different (not shown here). Wind spectra in Figure 7 are from the floating station, and show some similarity with those of the current (averaged over the whole sea). As already visible in the time series (Fig. 2), the north component of wind contains much more variance than the east component (Fig. 7, upper panels). To a lesser extent, this is also valid for the current. For the north component, current and wind show about the same frequency dependence ($\approx f^{-2}$) at periods shorter than 24 h.

In the rotary spectra of Figure 7 (lower panels), clockwise rotating currents are much more energetic around the inertial frequency than anticlockwise rotating currents. This is not valid for the wind, where both components contain about the same variance. The reason for this finding is obviously the presence of inertial waves. The broad spectrum may be explained by relatively short events of oscillations. In addition, damping may shift the actual inertial fre-

quency to values somewhat below f. The jagged appearence of the spectrum is in accordance with the statistical uncertainty, as expressed by the confidence limits.

Winds are strongly influenced by the diurnal warming and cooling and thus, a diurnal peak (24 h) was expected, but is present neither in the wind nor in the current spectra of Figure 7. Also the analysis of sea-level measurements from autumn 1984 (Sirkes, 1986) showed only a very weak diurnal signal. However, short-period oscillations were observed, which could be attributed to (barotropic) surface seiches. In agreement with numerical predictions, the sea-level spectra showed one distinct peak at about 34 min, the period of the first mode. Unfortunately, the 2 h sampling of the CODAR measurements does not permit resolution of this period. The spectral analysis of the current-meter data (not presented here) reveals some energy at frequencies above the Nyquist frequency of the CODAR time series, but no distinct peak. This high-frequency variance is relatively low and aliasing should affect only the high-frequency tail of the CODAR spectra (above about 0.15 h^{-1}). Indeed, the spectra of Figure 7 show some indication of this effect.

Empirical orthogonal eigenfunctions

Kundu and Allen (1976) extended the decomposition into EOFs to two-dimensional vector time series (described by complex numbers) and the analysis of horizontal current variability. Also, Denbo and Allen (1984) and Klinck (1985) have used this method.

The two-dimensional current field, as represented by complex numbers in (1), may be decomposed into EOFs by,

$$w_{li} = \sum_m a_i^{(m)} e_l^{(m)}$$

$$\text{with, } a_i^{(m)} = \sum_l w_{li} e_l^{(m)*} \qquad (4)$$

where l = 1, ..., M denotes the grid points, i = 1, ..., N is the time counter, and m ≤ M is the order of the EOF. Again, it is assumed that the w_{li} are of zero mean, *i.e.* the temporal mean has been subtracted for each grid point. The eigenfunctions $e_l^{(m)}$ are determined by the eigenvalue problem,

$$\sum_k C_{lk} e_k^{(m)} = \lambda^{(m)} e_l^{(m)}$$

$$\text{with, } C_{lk} = \sum_i w_{li} w_{ki}^* / N \qquad (5)$$

with C_{lk} being the M × M-covariance matrix of the complex currents. As this matrix is Hermitian, the eigenvectors $\lambda_l^{(m)}$ are mutually orthogonal and the eigenvalues $\lambda^{(m)}$ are real. They describe the ratio of total variance explained by the data,

$$\sum_m \lambda^{(m)} = \sum_k C_{kk} \qquad (6)$$

Figure 8 displays the first two EOFs of 75 grid points in the Dead Sea. These are the same grid points as used for the spectral analysis of the preceding chapter. The eigenvectors may be multiplied by an arbitrary complex number, *i.e.* only relative magnitudes and directions are of importance. The first two EOFs contain 53.7 % and 12.1 % of the variance, respectively. A separate analysis of the southern and northern half grid system yields the same EOF structure. The analysis may also be applied to certain frequency bands of clock- or anticlockwise rotation (Denbo and Allen, 1984). This has been done with the result that the 1. EOF is mainly due to clockwise rotating currents, in accordance with the spectral distribution in Figure 7. Anticlockwise EOFs show some different features but will not be discussed here because of their low variance.

The 1. EOF in Figure 8 is relatively homogeneous. Its contribution may be understood as the adjustment of currents to the mean wind. This interpretation is in accordance with the correlation analysis presented, which yields a (linearly) wind-driven portion of 42%, *i.e.* a value close to that accounted for by the 1. EOF. Already the 1. EOF contains some spatial variability, but most of it is represented by higher-order EOFs. The 2. EOF in Figure 8 somehow separates the northern and southern circulation as discussed before.

The two first EOFs account for only 66% of the variance, the third for another 8.1%, etc. Thus, it is not possible to explain the circulation in the Dead Sea by a few (*e.g.* three) flow patterns. In order to clarify this statement, Figure 9 presents the attempt to reconstruct the current field from Figure 3 (left panel). The left panel shows the mean current from the whole measuring period, with values mostly below 5 cm s^{-1}. The right panel presents the reconstruction by means of (4) with the first three EOFs. The current field is similar to that of Figure 3 but introduces considerable smoothing.

HORIZONTAL DERIVATIVES

The variability of surface currents may best be characterized by their horizontal derivatives and deduced values like divergence and curl. We briefly describe the method of computing derivatives and estimating their reliability. A more detailed presentation is given by Essen *et al.* (1988). We restrict our discussion to those aspects which are necessary to understand the error analysis used.

One radar station measures the radial current velocities with respect to its position. At least two radars at distinct sites are necessary to determine two-dimensional current vectors. For computing horizontal derivatives, the two-dimensional current velocities are approximated by first-order polynomials within a given circle around a certain grid point,

$$u = a_0 + a_1 x + a_2 y, \quad v = b_0 + b_1 x + b_2 y \qquad (7)$$

where the coordinates (x,y) refer to the grid point. From this approach, mean currents and first-order horizontal derivatives may be derived. Higher-order derivatives, which are not the subject of this paper, may be obtained by means of polynomials of respective order.

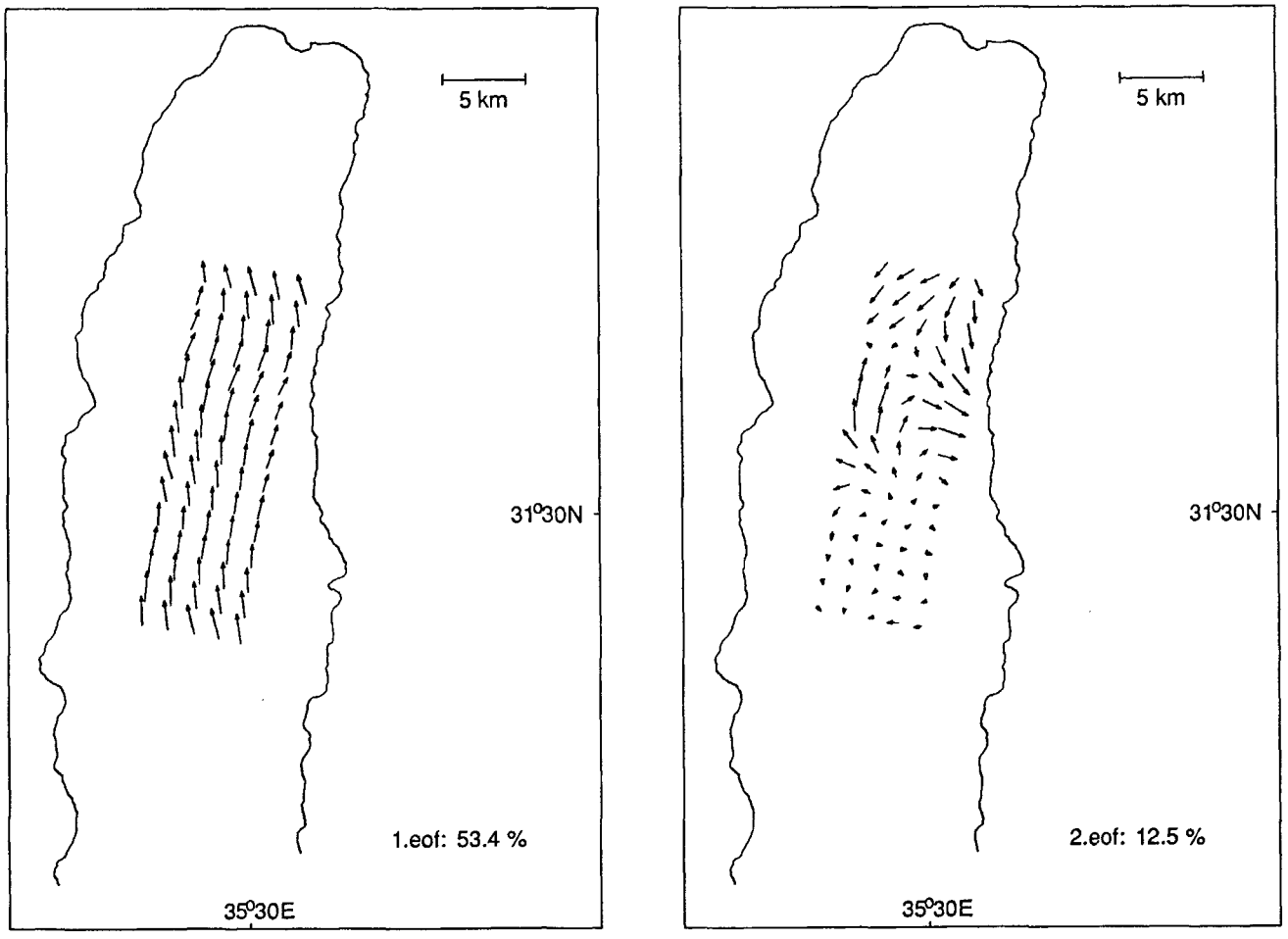

Figure 8

First and second horizontal EOF, arbitrarily normalized in amplitude and direction. The portions of variance are indicated.

The measured radial components depend on the two-dimensional current vector by,

$$u_r(x,y) = u(x,y)\sin\vartheta + v(x,y)\cos\vartheta \qquad (8)$$

where ϑ is the direction with respect to the radar site. Considering all radial velocities from both stations in the respective circle, the amplitudes a_l and b_l ($l = 0,1,2$) are determined by means of least-squares methods. The least-squares sum, which has to be minimized, is,

$$\varepsilon^2 = \sum_i g_i [u_{ri} \pm (a_0 + a_1 x + a_2 y)\sin\vartheta_i \pm (b_0 + b_1 x + b_2 y)\cos\vartheta_i]^2 \qquad (9)$$

The contributions to the least-squares sum are weighted by the respective signal strengths g_i The variance of the radial velocities with respect to the considered polynomials becomes,

$$\sigma^2 = \varepsilon^2 / \sum_i g_i \qquad (10)$$

The square roots σ found in the Dead Sea range from 5 cm s^{-1} to 10 cm s^{-1}. Apart from small variations, this value is independent of the order of the polynomial approach and the horizontal averaging area (circles of radius from 1.5 km to 5.0 km). The variances are partly due to the measuring system (radar noise and resolution in frequency and space), but there may also be a contribution from the spatial variability of currents. In estimating the errors of the polynomial amplitudes a_l and b_l, it is assumed that the covariance matrix of the radial velocities is diagonal, which means that the measurements are uncorrelated. The variance of the radial velocities (weighted by their signal strength) are considered as diagonal elements.

The least-squares algorithm yields the polynomial amplitudes. Current velocities and their horizontal derivatives depend linearly on the polynomial amplitudes. Their errors may be calculated from the covariance matrix of the amplitudes. Errors are estimated in dividing the respective rms-values by the square root of the number of contributing radial velocities, which is an optimistic estimation. The error of the mean radial current, averaged within a circle of 2 km radius, is of the order of 1 cm s^{-1}. In the case of optimal geometry, that means positions with radial directions of both stations perpendicular to each other, the errors of both components of the two-dimensional current vector are the same. By increasing the averaging circle the error decreases proportional to the radius.

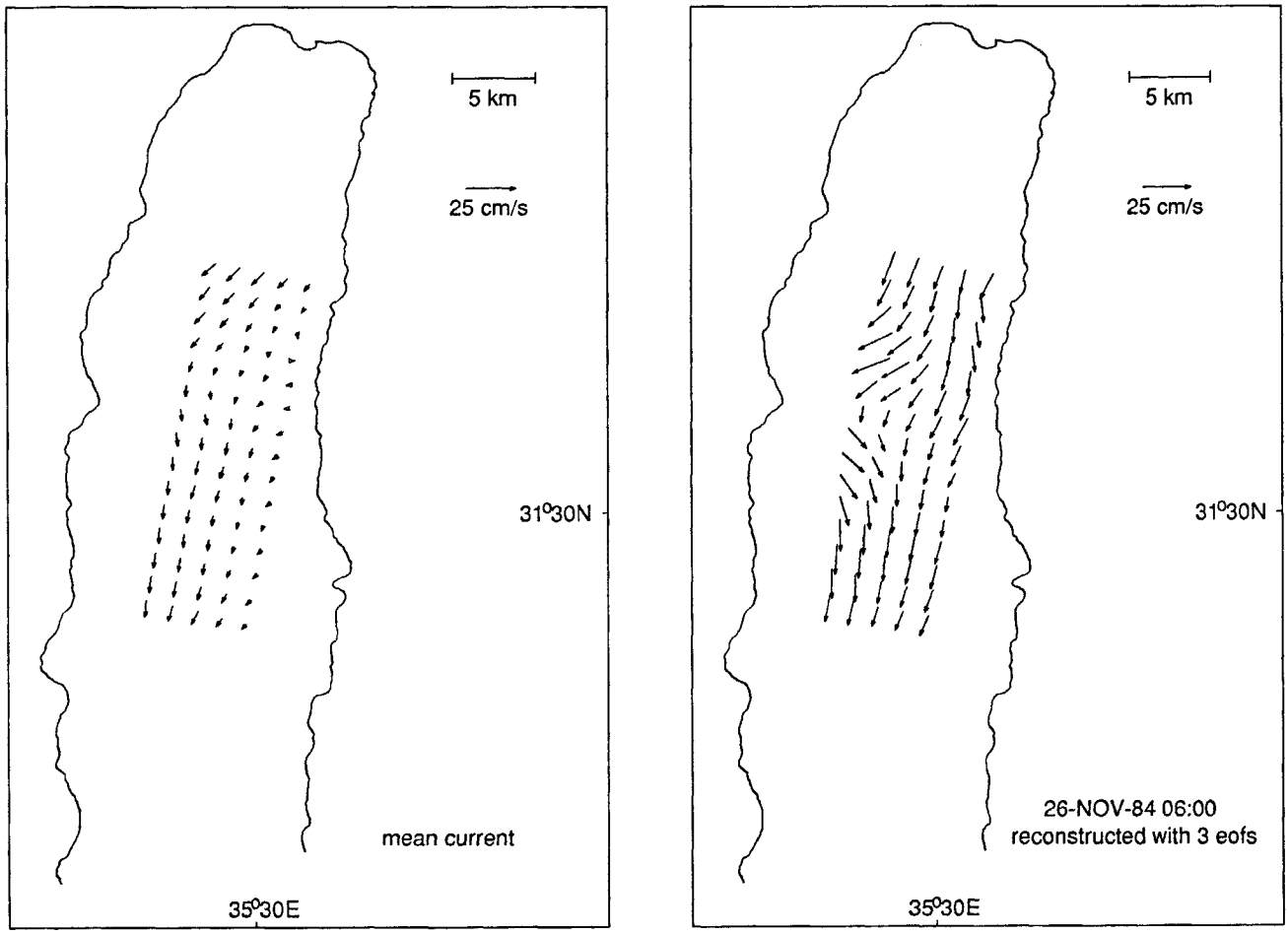

Figure 9

Mean current (left panel) and the portion of current from Figure 3, as represented by the first three EOFs (right panel).

Divergence, curl, stretch, shear

In the case of estimating first order derivatives from first order polynomials, we obtain four amplitudes which are related to the commonly used quantities by,

$$\left.\begin{aligned} &\text{divergence: } \partial u/\partial x + \partial v/\partial y = a_1 + b_2 \\ &\text{curl: } \partial v/\partial x \pm \partial u/\partial y = b_1 \pm a_2 \\ &\text{stretch: } \partial u/\partial x \pm \partial v/\partial y = a_1 \pm b_2 \\ &\text{shear: } \partial v/\partial x + \partial u/\partial y = b_1 + a_2 \end{aligned}\right\} \quad (11)$$

The error analysis shows that errors of these quantities depend more strongly on the averaging radius than the current velocities do. This effect can be explained by the error propagation in differences, as used for computing derivatives. Though there is a certain variability due to the data quality, some general results may be stated. An averaging radius of 2 km yields errors of the order of the quantities themselves. Increasing the averaging radius to 5 km, the error decreases by a factor 5 and more, yielding a reasonable signal-to-noise ratio.

Figure 10 shows time series of divergence, curl, stretch, and shear. The averaging circle (5 km) is shown in the map. The scale used is the local Coriolis number,

$$f = 7.5 \times 10^{\pm 5} s^{\pm 1} \quad (12)$$

Time series from other areas look quite different. In the case of smaller averaging circles the absolute values of the considered quantities become larger. As additional examples show (not presented here), this is a general feature. Also, averaging areas only few kilometres apart show different results. One conclusion could be that noise dominates. But this seems unlikely because of the error estimation presented and the behaviour of the time series, which show a high reproducibility over several hours. Thus, it can be concluded that the scale of horizontal variability is smaller than our averaging circle of 10 km in diameter.

Obviously, the average divergence, curl, stretch, and shear are considerably smaller than f. But this is not always the case. Especially for smaller averaging circles and in the northern part of the lake, all of the four quantities may reach values of the order of f. In general, the divergence is small in Figure 10. Between 26-Nov. and 29-Nov., it is

negative nearly all the time, indicating downwelling in the southern part of the Dead Sea. This is in accordance with strong surface currents directed to the south for the respective period (cf. Fig. 5) and the necessary recirculation. Also in the other parts of the lake, the average divergence is small, except for special periods with upwelling dominating in the northern part of the lake. With the exception of some short periods, the curl is positive in Figure 10, indicating the presence of cyclonic gyres. A similar behaviour has been found for the central lake, while in the northern part the curl is positive for the first four days of the experiment and changes sign several times afterwards.

Acceleration

Figure 11 compares acceleration terms of the Navier-Stokes equation. For this purpose the following ratios are defined,

$$\left.\begin{aligned} &AC = (|b_u / b_t|, |b_v / b_t|),\ RO = (|b_u / b_f|, |b_v / b_f|), \\ &\text{with, } b_u = u\ \partial u/\partial x + v\ \partial u/\partial y,\ b_v = u\ \partial v/\partial x + v\ \partial v/\partial y \\ &b_t = ((\partial u/\partial t)^2 + (\partial v/\partial t)^2)^{1/2},\ b_f = f\ (u^2 + v^2)^{1/2} \end{aligned}\right\} \quad (13)$$

The horizontal derivatives are obtained as before. The temporal accelerations are computed by means of central differences with a time lag of twice the sampling time. This procedure is sensitive to numerical instabilities and, in fact, some single values do not fit to adjacent ones (cf. Fig. 11, upper two time series). Nevertheless, most of the data show a reliable behaviour and allow an estimation of the order of magnitude of the temporal acceleration.

The ratio AC is a measure of the nonlinearity of the water motion. In the averaging area considered, the ratio of temporal (linear) to horizontal (nonlinear) acceleration is below 0.5. This is true for the whole lake. There is no obvious difference between the east- and north-components, as could be expected because of the geometry of the Dead Sea. With smaller averaging areas (2 km radius), values of the order 1 occur, but also the number of noisy data increases, and a reliable estimation becomes difficult. The smaller the scales considered, the higher is the nonlinearity.

The Rossby number RO (cf. Fig. 11, lower two time series) is of the order 0.3 and less, and there is no distinct difference between the two components. The Rossby number shows similar behaviour within the whole lake, but without correlation between data from positions several kilometres apart. With a smaller averaging radius (2 km), the Rossby number can reach values of the order of 1, *i.e.* in some cases nonlinear effects may be as impor-

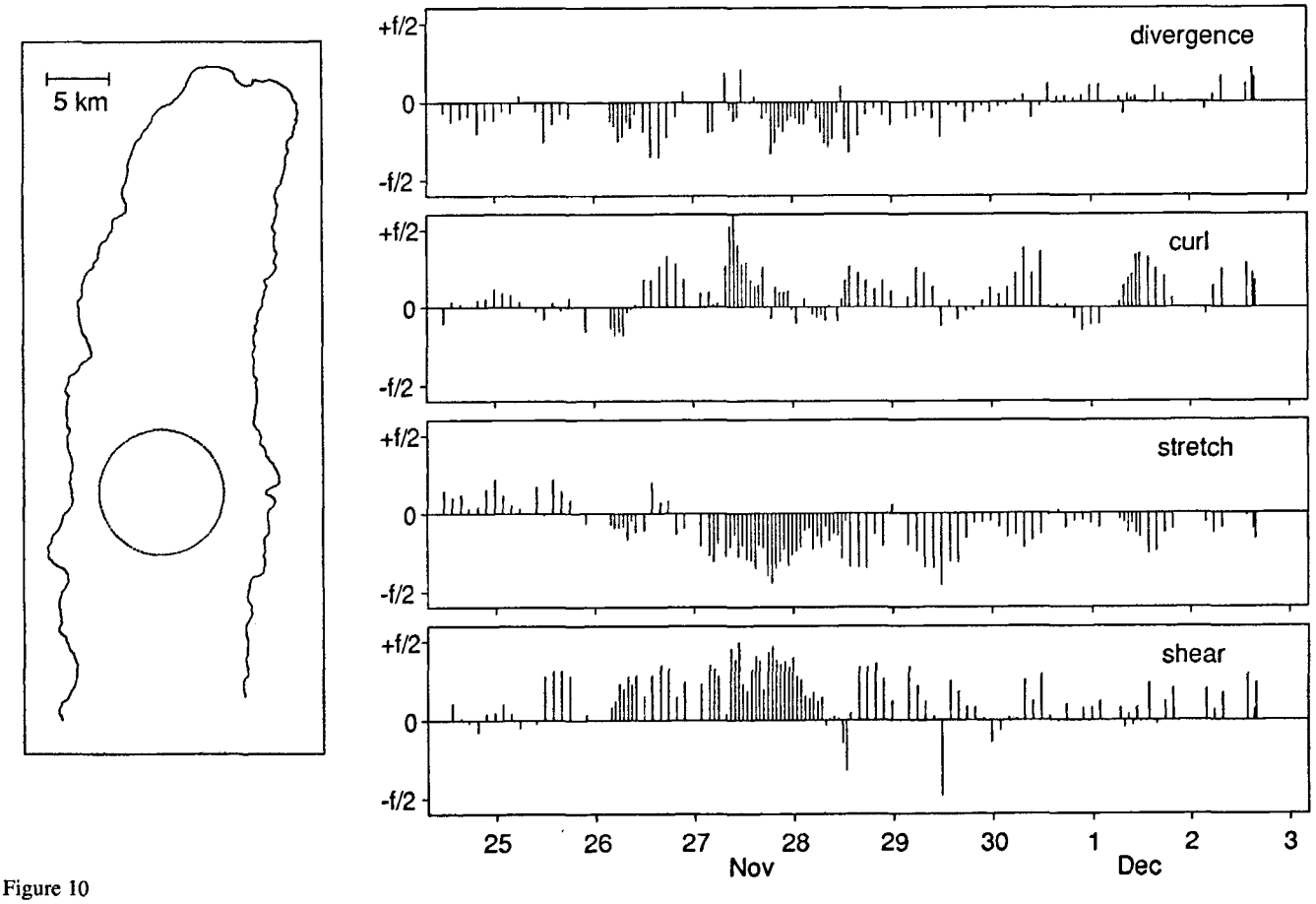

Figure 10

Time series of divergence, curl, stretch, and shear. The dashed circle in the map (5 km radius) is the averaging area.

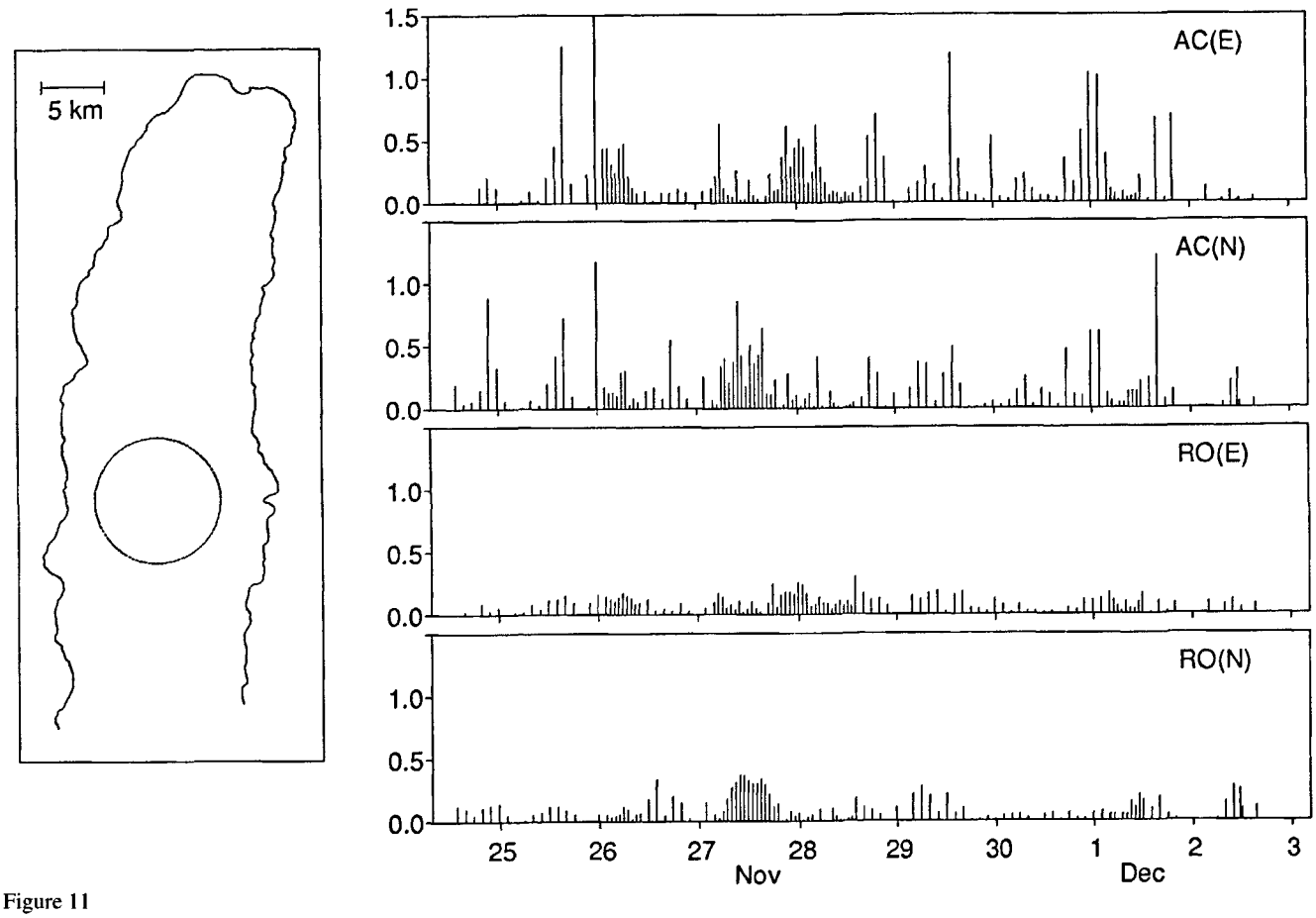

Figure 11

Time series of east-(E) and north-component (N) of acceleration ratios, as defined by (13): nonlinear-to-linear (AC), nonlinear-to-inertial (RO). The dashed circle in the map (5 km radius) is the averaging area.

tant as the Coriolis force but in general, the Coriolis force dominates.

CONCLUSIONS

Only HF radar permits determination of the spatial variability of surface currents with a resolution of a few kilometres. This technique makes use of the ground wave, which propagates over conductive water only. The Dead Sea is one of the few inland seas fulfilling this requirement.

The data set presented allows both the analysis of time series at various grid points and the investigation of flow patterns at a given time. By means of vector-correlation techniques it has been found that about 45 % of the current variance can be explained by linear wind forcing. Rotary spectral analysis provides evidence of the presence of events of inertial oscillation.

As the result of an EOF analysis it may be stated that current fields in the Dead Sea cannot be represented by a small number of flow patterns.

Strong changes in both current speed and direction occur on scales of only a few kilometres. For an averaging radius of 5 km, the curl reaches values of $f/2$, the divergence of $f/4$ and the Rossby number of 0.3. From selected maps of low noise it has been found that these values may be exceeded by about a factor of 2 for the smaller averaging radius of 2 km. In addition, the comparison of the temporal and advective acceleration proves that nonlinear processes are important.

Acknowledgments

Our special thanks are extended to Professor J.R. Gat for his help and advice throughout this research. We thank Professors J. Stanhill and A. Cohen, the Israël Meteorological Service and the Israeli Navy for the wind data and Dr. D.A. Anati for hydrological data. R. Cordlandwehr, T. Freygang, and M. Hamann helped in performing the experiment. Thanks go to Dr. M. Bohle-Carbonell for helpful suggestions. This work was supported by the Israel Ministry of Energy and Infrastructure under Contract 1828, by a grant of the Mediterranean-Deep Sea Company and by the German Science Foundation (DFG, Sonderforschungsbereich 94).

REFERENCES

Anati D.A. (1984). Personal communication.

Barrick D.E., M.W. Evans, B.L. Weber (1977). Ocean surface currents mapped by radar. *Science* **198**, 138-144.

Denbo D.W., J.S. Allen (1984). Rotary empirical orthogonal function analysis of currents near the Oregon coast. *J. Phys. Oceanogr.* **14**, 35-46.

Essen H.-H., T. Freygang, K.-W. Gurgel, F. Schirmer (1984). Oberflächenströmungen vor Sylt - Radarmessungen im Herbst 1983 - *Dt. Hydrogr. Z.* **37**, 201-215.

Essen H.-H., K.-W. Gurgel, F. Schirmer (1988). Horizontal and temporal variability of surface currents in the «Lubecker Bucht», as measured by radar. *Dt. Hydrogr. Z.* bf **41**, 57-74.

Essen H.-H., K.-W. Gurgel, F. Schirmer (1989). Surface currents in the Norwegian Channel measured by radar in March 1985. *Tellus* **41**A, 162-174.

Essen H.-H (1993). Ekman portion of surface currents, as measured by radar in different areas. *Dt. Hydrogr. Z.* **45**, 57-85.

Klinck J.M. (1985). EOF analysis of Central Drake Passage currents from DRAKE79. *J. Phys. Oceanogr.* **15**, 288-298.

Kundu P.K., J.S. Allen (1976). Some three-dimensional characteristics of low-frequency current fluctuations near the Oregon coast. *J. Phys. Oceanogr.* **6**, 181-199.

Sirkes Z. (1986). Seiches and currents in the Dead Sea. Ph.D. thesis, Weizmann Inst. of Science, Rehovot, Israël., 66 p.

Sirkes Z. (1987). Surface manifestations of internal oscillations in a highly saline lake (the Dead Sea). *Limnol. Oceanogr.* **32**, 76-82.

Sirkes Z., F. Schirmer, H.-H. Essen, K.-W. Gurgel (1995). Surface currents and seiches in the Dead Sea. In: T.M. Niemi, Z. Ben-Avraham, and J. Gat (eds.). The Dead Sea - a summary of recent research. Oxford University Press, (in press).